ISSN 8755-6839

SCIENCE OF **TSUNAMI HAZARDS**

Journal of Tsunami Society International

Volume 39 **Number 3** **2020**

RADAR SUBSYSTEMS OF AUTONOMOUS MOBILE ROBOTIC SYSTEMS FOR STUDYING TSUNAMI IN THE COASTAL ZONE

P. Beresnev, A. Kurkin, A. Kuzin, A. Myakinkov, E. Pelinovsky, A. Ryndyk, S. Shabalin

Nizhny Novgorod State Technical University n.a. R.E. Alekseev, Nizhny Novgorod, RUSSIA.

ABSTRACT

The problems of using robotic systems for survey and registration of tsunami tracks in hard-to-reach places are discussed. The description of such a complex with good operational characteristics, developed at the Nizhny Novgorod State Technical University n.a. R.E. Alekseev is given. A solution is presented that allows to equip an autonomous mobile robotic complex with a sensor of the own production and increase its cross-country ability. A method for constructing an antenna array, which allows achieving optimal characteristics in terms of maximum detection range and angular resolution is proposed. This result is achieved due to the fact that the entire geometric aperture of the antenna is "filled" with elements (columns) with an array pitch of half the wavelength. In this case, the placement of the receiving sub-arrays at the edges of the substrate forms the largest aperture under the conditions of the problem been solved and allows the use of the classical method of beam-forming when working in the far zone. An example of constructing an antenna array providing the formation of beams with a width of 5° in the sector of the far-field angles is considered. Application of the proposed solution allows you to expand the detection area of objects.

***Keywords**: coastal monitoring, marine hazards, autonomous mobile robot, radar, antenna array*

1. Introduction

In this century, the tsunami problem has come to the fore, resulting in the highest number of casualties compared to other natural disasters. Fifteen years ago, the strongest earthquake in the Indian Ocean around the coast of Indonesia on December 26, 2004 with a magnitude of 9.3 led to a tsunami that turned out to be devastating for many countries in the Indian Ocean and led to the death of about 300 thousand people [1-5]. An earthquake of March 11, 2011 off the coast of Japan with a magnitude of 9.0 caused a tsunami with a maximum height of about 40 m and led to a technological disaster: the destruction of the Fukushima nuclear power plant [5-9]. On average, a global tsunami occurs almost every month, but only one in ten (about once a year) causes damage. The highest height on land that the tsunami wave reached in the post-war years is 524 m; it happened on July 9, 1958 in Alaska, when a giant landslide with a volume of about 80 million cubic meters descended from the slopes of Mount Fairweather into Lituya Bay [10]. National and international tsunami warning services have been established, and their effectiveness is increasing all the time (especially in forecasting distant tsunamis). Now the forecasting of the tsunami and its consequences has become a practical matter: plans for evacuations are communicated to residents, training of the population is arranged, protective devices are being built, etc.

The tsunami also does not bypass Russia. The most destructive in post-war history was the tsunami on November 4-5, 1952, when a wave with a height of about 10 m caused significant damage to the city of Severo-Kurilsk on the Paramushir Island, and many of its inhabitants died [10, 11]. In this century, several large tsunamis happened in the Russian Far East. Thus, a tsunami 2 m high was recorded on Sakhalin during the 2007 Nevelskoye earthquake [12, 13]. The Kuril tsunamis that occurred on November 15, 2006 and January 13, 2007, were over 10 m high and caused damage on the American coast [14-16]. Distant tsunamis that came from Samoa in 2009 and Chile in 2010 were also recorded by Russian stations [17]. Finally, the 2011 tsunami led to the breaking of the ice cover in the Kuril Islands [9].

Tsunamis occurred not only in the Russian Far East. About 20 tsunami events were registered in the Black Sea [18-20], and about 10 - in the Caspian Sea [21]. Tsunami-like phenomena also occur in inland water bodies of Russia: on rivers, lakes and reservoirs [22-24]. To understand the physics of tsunamis and to develop methods to mitigate tsunami damage, it is essential to have reliable data on the characteristics of tsunamis onshore. Survey of tsunami trails is usually carried out after all devastating tsunamis, as a rule, by national teams and using various methods. Since the 1992 tsunami in Bali (Indonesia), many tsunamis have been surveyed by international expeditions, which contributed to the development of uniform standards for conducting such expeditions and a list of characteristics that must be obtained during the survey. This experience is summarized in [25]. One of the authors of this article (Pelinovsky E.N.) began to take part in international tsunami expeditions since 1993 (Okushir tsunami in the Sea of Japan), and the experience gained is reflected in publication [26]. During the survey, an interrogation of the population is usually carried out, as well as measurements of the visible traces of the tsunami (run-up and wave heights, time of arrival, number of waves, polarity of waves). However, as a rule, the expedition manages to reach the place a week or two after the event that has already happened, when some of the tsunami witnesses

some of the visible traces of the tsunami disappear due to storms and rains, as well as during have already left the area of the disaster and restoration work. Nevertheless, the data obtained during the expedition are invaluable and are the main source for further actions to improve the methods of tsunami prediction.

Over the past 20 years, new tsunami survey techniques have begun to be developed that provide tsunami data in hard-to-reach areas or better plan tsunami expeditions. In particular, aerial photography from helicopters and drones has now begun to be used to survey tsunami traces over a vast area, see, for example, the article on the survey of the tsunami on the island of Sulawesi in 2018 [27]. Another area of study of tsunami traces in hard-to-reach places is the use of autonomous mobile robotic systems used in our team.

This present article describes an autonomous mobile robotic complex with good performance characteristics, developed at the Nizhny Novgorod State Technical University n.a. R.E. Alekseev. A solution is presented that allows to equip it with a sensor of our own production and increase its cross-country ability. A method for constructing an antenna array is proposed, which makes it possible to achieve close to optimal characteristics with respect to the maximum detection range and angular resolution.

2. Brief information about the autonomous robotic complex

One of the examples of robotic systems for monitoring the situation in the coastal zone is an autonomous mobile robotic complex (AMRK) [28-31], developed by the research team of the NNSTU n.a. R.E. Alekseev. This complex is equipped with a shipborne radar MRS-1000 (speed of a circular view of space from 12 to 24 rpm, operating frequency range from 9300 to 9500 MHz, transmitter power adjustment range of 28 dB, device protection degree IP65), a LIDAR LMS511Pro light detection system, video camera AXIS Q6045-E, differential positioning system GPS / GLONASS OS-103 (positioning error in motion mode not more than 30 cm) and weather station Vaysala WX520 (Fig. 1).

An autonomous mobile robotic complex (Fig. 1) is capable to carry out continuous monitoring of the coastal zone in any climatic conditions and on any type of support base due to the possibility of installing three different types of movers. The wheeled mover is designed for use on hard soil, as well as in dry and wet soils. The caterpillar type of mover allows you to increase the efficiency of the complex when driving in hard-to-reach places, such as sandy terrain, wet soils, snow. The rotary-screw type of mover device can be used to operate in swamps and flooded areas.

In May-June 2016 on the coast of Sakhalin Island, field tests of an experimental AMRK were carried out. The purpose of the experimental research on the coast of Sakhalin Island was to evaluate the effectiveness of the AMRK functioning and to perform typical maneuvers to study the mobility of the developed chassis. On the basis of experimental research by a team of performers, it was concluded that a number of constructive measures must be taken to increase the mobility of the complex and the effectiveness of the tasks assigned.

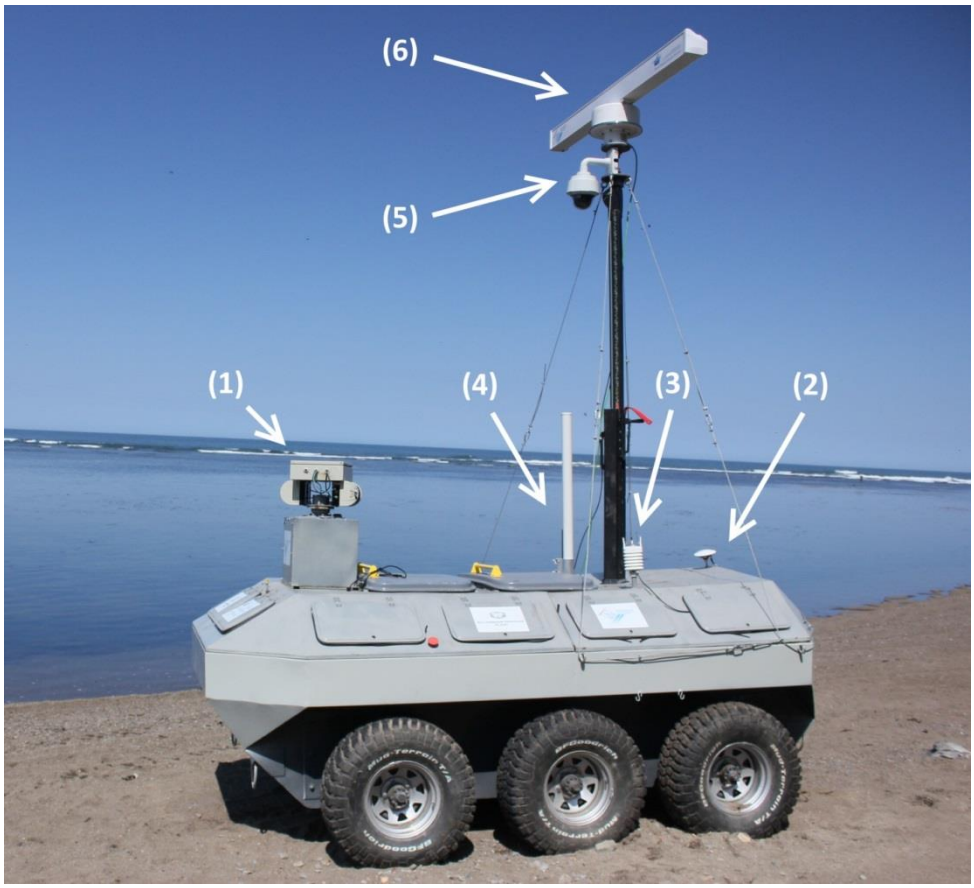

Fig. 1. Autonomous mobile robotic complex: 1 – LIDAR LMS511Pro;
2 – OS-103 positioning system antennas; 3 – Vaysala WX520 weather station;
4 – Rocket M2 omnidirectional Wi-Fi antenna; 5 – AXIS Q6045-E video camera;
6 – MRS-1000 circular view radar

The first one concerns with the development of an independent adaptive suspension. Currently, AMRK does not have a suspension, which limits the operation of the complex on hilly and mountainous areas, and also increases the risk of damage to expensive measuring equipment both as a result of the AMRK overturning and as a result of shock loads transmitted through the chassis body. Also, during the tests, it was revealed that one of the problems in creating autonomous systems is the need for automatic route correction. A deviation from the course can be the result of several reasons, including the heterogeneity of the soil, its viscosity, and massive obstacles along the way. Feedback control is required to implement the route correction system. Control with feedback is required to implement the route correction system. Such a system should include a radar system, which is currently considered as one of the key technologies for automated piloting of vehicles [32, 33].

3. Existing approaches to the construction of antenna arrays of radar systems

The most important task in the design of a radar system is the development of an antenna. The task of optimizing the architecture of the antenna system becomes especially urgent in the case of designing small-sized radars, when restriction on the geometric dimensions is one of the determining factor. Such radars include automotive radars, which are the object of analysis in this work. Antenna arrays (AR) are almost always used in the structure of modern automobile radars. It is caused by the flexibility of digital formation of the specified directivity characteristics, which is necessary to implement the required radar operating modes. The complexity of their design is determined by the contradictoriness of the requirements. In order to form a narrow beam of the directivity pattern (DP) providing the required angular resolution, corresponding antenna aperture is required. To provide unambiguous measurement of the angular coordinates within wide sector (so called near region from 90 to 120 degrees) we should exclude the arising of interference maximums of DP. In this case, we should provide the number of equivalent receive channels corresponding to the quantity of elements placed with the pitch of the half wavelength.

There are two traditional ways to solving this problem. First one is using of separated receive channels for each element of the array. For example, to ensure the beam width of the receiving antenna in azimuth of five degrees, sixteen to twenty array elements are required, depending on the weight function that determines the level of the side lobes. The requirement associated with cost reduction defines restrictions of the number of receiving channels, since not only the complexity and number of receiving and transmitting modules, but also the number of ADCs, the required throughput, and the performance of the digital processing system depend on the number of receiving channels. In practice, the number of receiving channels in the automotive radar should be either less than the number of array elements, or the array should be sparse. The construction of a sparse antenna array, when the distance between the elements (columns) significantly exceeds half wavelength, leads to energy losses compared to filled arrays. In addition, interference lobes are formed in the directivity pattern.

The second and widely used approach is use of MIMO (Multiple Input Multiple Output) technology [34]. In this case, radiation and the corresponding coherent processing of orthogonal signals help to exclude the interference maximums, but the losses associated with

the sparseness of the aperture remain. However, in some cases, automotive radar developers use this approach [35, 36] if energy requirements are not critical. This situation may occur when building medium and short range radars (up to 100 m).

4. Optimization of the structure of the radar antenna array

The most suitable for building the required antenna array from the point of view of maintaining the number of elements and reducing the number of channels is the option associated with combining columns into subarrays. In this case, the antenna aperture can be completely filled with the elements, but the distance between phase centers can be several times greater than the wavelength. This ideology is inherent in most modern long-range radars.

A schematic representation of the antenna aperture of an automotive radar is shown in Fig. 2. Suppose that there is a restriction on the total size of the antenna array, and its maximum width is determined by L_A. One part of this aperture L_{tr} can be used to place elements of a transmitting antenna, another part L_{rc} can be used for receiving array. The vertical size of the transmitting and receiving antennas $H_{tr,rc}$ can be different, for example, due to the peculiarities of the placement of integrated transceiver modules on the substrate and the tracing of the feed lines.

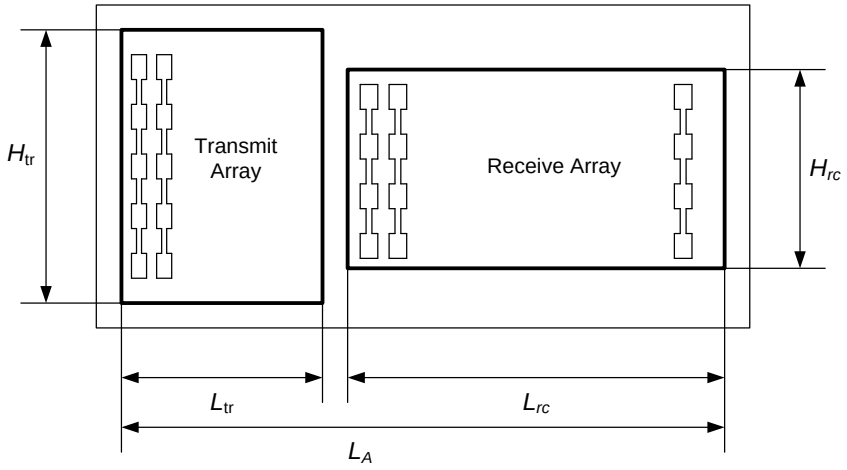

Fig. 2. Illustration for calculating the optimal ratio of the aperture sizes of the transmitter and receiver

In accordance with the basic radar equation [38], the signal power at the output of the receiving antenna of the radar is proportional to the product of the gain of the transmitting antenna G_{tr} and the effective aperture area of the receiving antenna A_{rc}:

$$P_{rc} \sim G_{tr} A_{rc}. \quad (1)$$

It is known, that the gain of a flat aperture is determined by the ratio of its effective area to the square of the wavelength ($G_{tr} = 4\pi A_{tr} / \lambda^2$), as well as the fact that the effective area of the

apertures is proportional to their geometric area (accurate to the utilization factor), which is equal to the transmitting and receiving antennas respectively $S_{tr} = H_{tr} L_{tr}$, $S_{rc} = H_{rc} L_{rc}$, we see that the output power of the receiver will be maximum when the product ($H_{tr} L_{tr}$) ($H_{rc} L_{rc}$) is maximal. According to Fig. 2, $L_{rc} \approx L_A - L_{tr}$. Then, in order to maximize the power entering the receiver, with the given restrictions on the height of the apertures, it is necessary that the condition for maximizing the product $L_{tr} (L_A - L_{tr}) = L_{tr} L_A - L_{tr}^2$ is fulfilled. To determine the maximization condition, we equate to zero the derivative of this expression with respect to L_{tr}. As a result, we obtain a simple ratio:

$$L_{tr|Ptr = max} = L_A/2. \quad (2)$$

Thus, regardless of other factors, the maximum range of the radar with the antenna configuration under consideration, while maintaining its total geometric area, will occur when the total antenna aperture is divided equally between the transmitting and receiving antennas. Figure 3 shows the results of calculating the signal-to-noise ratio at the input of an automotive radar receiver when a signal is reflected from a target with an effective scattering area of 0.2 m^2 at a distance of 100 m when using the 77 GHz FMCW radar. The frequency deviation is assumed to be equal to 200 MHz, the radiated power is 20 mW, the noise coefficient of the receiver is 13 dB, the total aperture size is L_A = 14 cm.

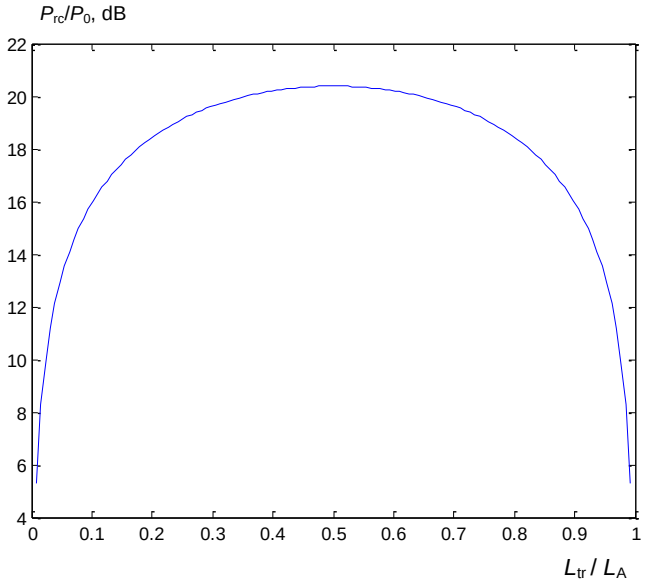

Fig. 3. Dependence of the signal-to-noise ratio at the receiver input on the relative size of the transmitting antenna

It can be seen from the graph in Fig. 3 that the value of the signal-to-noise ratio at the receiver input, which has a maximum at $L_{tr} = L_A/2$, decreases slowly when the area ratio changes, up to the values when the aperture of one of the antennas is not more than 0.2 of the total aperture.

It should also be noted that with a parallel method of irradiating the viewing sector, the beam width of the transmitting array should not be less than the width of this sector itself. A typical value of the width of the radar sector of view in the far zone is 12 ... 15 degrees. At the same time, while the columns of the transmitting antenna are spaced with a pitch equal to half of the wavelength, there is no sense to use more than eight…ten columns for transmission in the far zone. Thus, if the requirements in respect to the whole aperture allow the total number of columns to be more than 16, it is worthwhile to use additional array columns to receive the signal.

The angular resolution is determined by the width of the main lobe of the spatial ambiguity function [39], which coincides with the antenna directivity pattern as function of the angular coordinate α if antenna is matched with the direction to the source of reflection. The directivity pattern of a transceiver antenna is calculated as a Fourier transform of the amplitude-phase distribution of the field along its aperture:

$$\Phi(\alpha) = \int_{-L_A/2}^{L_A/2} U_A(x) e^{j2\pi x \sin\alpha/\lambda} dx\,, \tag{3}$$

where L_A – antenna aperture size.

In the case under consideration, the amplitude-phase distribution $U_A(x)$ should be understood as the convolution of the field distributions over the aperture of the transmitting array $U_{tr}(x)$ and the receiving array $U_{rc}(x)$:

$$U_A(x) = \mathrm{conv}\{U_{tr}(x), U_{rc}(x)\}. \tag{4}$$

The beam width Δα of the antenna DP Φ(α) determined by (3) is defined by the ratio of the wavelength to the antenna aperture:

$$\Delta\alpha = k\lambda/(L_A \cos\alpha), \tag{5}$$

where coefficient k depends upon the character of function $U_A(x)$.

For the case of uniform amplitude distribution $k \approx 0.8$. This is easily illustrated by the example of linear antenna aperture. When its length is equal to one wavelength, the beam width is approximately equal to π/4 by the half power level and strongly to π/2 by between zeros. This coefficient falls when the distribution $U_A(x)$ has maximal values at the bounds of the aperture and rises when in the middle. The same time, distribution providing minimizing the beam width, follows to the rising of side lobes of DP.

In the case when the apertures of the transmitting and receiving antennas are the same, the function $U_A(x)$ has a accented maximum and monotonically decreases relative to this maximum. For example, with a uniform field distribution $U_A(x)$ has the form of a triangle. Such a form of this function is disadvantageous from the point of view of minimizing of

coefficient k in (5). To decrease k, it is desirable that the function $U_A(x)$ grows to the edges of the aperture, or at least remain uniform. While maintaining the "integrity" of the transmitting and receiving apertures, this is possible if the size of one of them is minimal, and the other, on the contrary, occupies a large part of the antenna aperture. This situation corresponds to the case when, for example, the transmitter is built on the basis of small number (for example, one or two) columns of the antenna array, and the receiving part of the antenna contains the maximal number of columns. Figure 4 shows the dependence of the beam width of the resulting directivity pattern of the transmitting and receiving arrays depending on the ratio of the size of the transmitting aperture to the total size of the antenna. This graph is built for the radar with the same parameters as the graph in Fig. 4.

Figure 4 demonstrates that the beam width with the maximum use of the antenna aperture for the receiving channels is less than the maximum beam width with an equal distribution of the aperture between the transmitter and receiver channels by about 1.4 times.

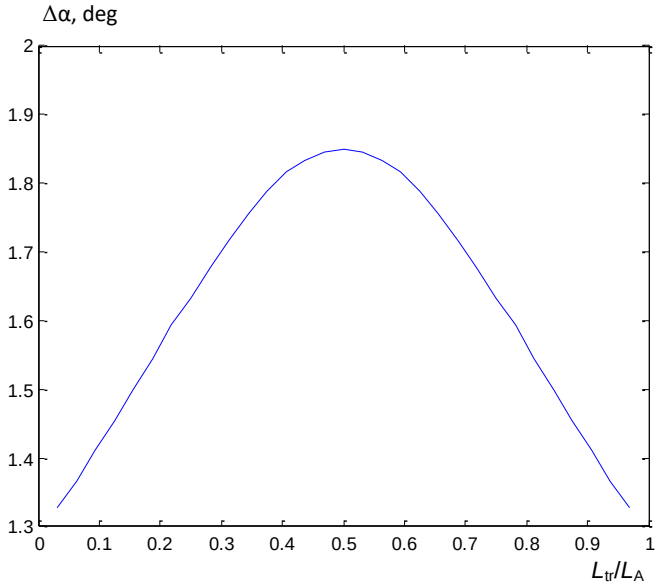

Fig. 4. Dependence of the beam width of the resulting beam on the ratio of the width of the aperture of the transmitter and the entire aperture

Thus, we see that the conditions under which the maximum range of the radar and the best resolution are achieved are contradictory.

To simultaneously satisfy the requirements of maximizing the range of the radar and high angular resolution, it is necessary, on the one hand, to maintain the quasi-equal distribution of the transmit and receive apertures, on the other hand, to place the extreme elements of one of them at a maximum distance from each other. Such a "compromise" solution could be realized placing either transmitting or receiving elements at the edges of the aperture. Holding the area of the aperture actually means holding the number of elements of the array along the horizontal (azimuthal) coordinate, that is, the number of columns. It is important to remember

that, despite the narrowing of the beam, such arrangement of the elements does not increase the gain (directivity) of the antenna, since part of the energy is radiated (received) in the direction of interference beams. The appearance of interference lobes, being a fee for narrowing the main beam of the directivity pattern, leads to the need to analyze the optimal method for placing array columns and choosing the optimal weight coefficients.

There are various ways to suppress side lobes and increase gain which are considered in many articles [40-42]. The basis for the suppression (partial suppression) of the arising interference lobes of the transmitter (receiver) DP is multiplication by a narrow directivity pattern, on the contrary, of the receiver (transmitter). Good suppression of interference lobes is possible using MIMO [43].

4.1. *Topology with sparse transmitters*

One of the possible methods of constructing a transmission array, providing the aperture size increasing, is placing of transmission subarrays at the maximum distance from each other. Consider the structure of the microstrip antenna array shown in Fig. 5 (1, 2-transmitting elements, 3-receiving elements).

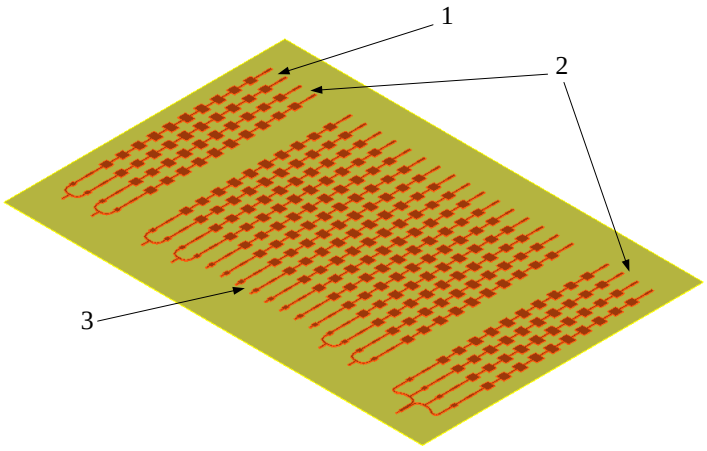

Fig. 5. Antenna array structure

The transmitting columns are located on the edges of the substrate, thereby forming the maximum possible aperture of the transmit antenna, while the receiving columns fill the space between the transmitters. In this structure transmitting elements 1 and 2 are used to irradiate the far zone. In the near zone only one transmitting subarray 1 is used to provide wide radar sector of view. Also, to eliminate influence of the interference maximums in the near zone, only eight “uncombined” elements of the receiving antenna array 3 are used. The phase of one of the transmitting channels takes the values of 0 degrees and 180 degrees, while the phase of the other transmitting channel is always equal to 0 degrees. With the antiphase switching on, the number of beams is the same, but a set of beams is orthogonal to the first one. This is illustrated by Fig. 6.

The implementation of this approach provides covering the observation sector in two sequential tacts of the transmitting arrays 1 and 2 for far zone and in one tact of transmitting array 1 for near zone. The distance between the phase centers of the transmitting subarrays is much greater than the wavelength. This circumstance determines the presence of a large number of interference lobes. The quantity and position of these lobes are determined by the distance between the transmitting elements. With the previously described geometric parameters of the phased antenna array, the repetition period of the interference lobes is approximately 11°, while the beam width is about 5°.

The most appropriate technique of constructing a receiving array taking into account both the requirements in respect to the maximizing its aperture and minimizing the number of receiving channels is use of subarrays formed of two or more columns. Figure 7 shows the receiving (curve 1), transmitting (curve 2) and resulting (curve 3) directivity patterns of the antenna during beam formation in various directions for far and near zones.

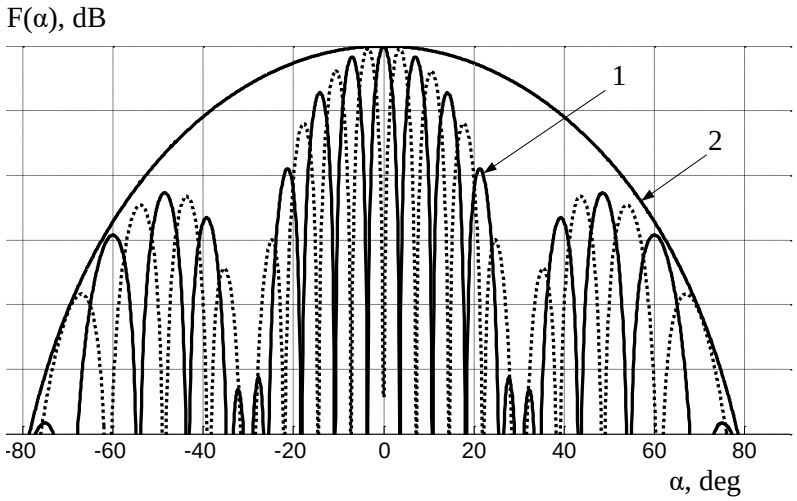

Fig. 6. Two orthogonal sets of beams of a transmission array consisting of two subarrays spaced apart at the edges of the aperture for far zone (1) and directivity pattern of the transmitting array for near zone (2)

As can be seen from Fig. 7, the resulting DP has the single main maximum that provides an unambiguous measurement of the angular coordinates. The reduction of the side lobes presents the special task which is solved by the optimization of digital beam forming.

The main disadvantage of the considered approach is the absence of the flexibility in respect to the forming of resulting beams of transceiver array. We can form receive and, therefore, resulting beams only in fixed directions of transmit beams. The same time, scanning of the observation sector with the pair of spread transmitters leads to the energy losses in comparison to the parallel irradiation of the same sector. This is caused by that loss-free scanning is possible only for the case when the gain of the scanning beam is *N*-times bigger than the gain of wide-radiating beam irradiating the whole sector. The number *N* is equal to the ratio of the

duration of the signal integration interval for the case of parallel observation to the duration when scanning, in acceptance that the whole sector observation time is the same. The same time, the gain of the pair of spread transmitters is only equal to the gain of "filled" transmitter consisting of the same quantity of elements and irradiating the whole sector.

4.2. *Topology with sparse receivers*

Achieving a high angular resolution with unambiguous azimuth measurement is also possible using the phased antenna array with maximally spaced fragments of the receiving array. This is achieved by the placing elements of receiving array, united into subarrays, at the edges of the general aperture simultaneously with placing of other elements in the central part. The middle part of the central fragment should have separated channels for each element, while side elements could be united into subarrays.

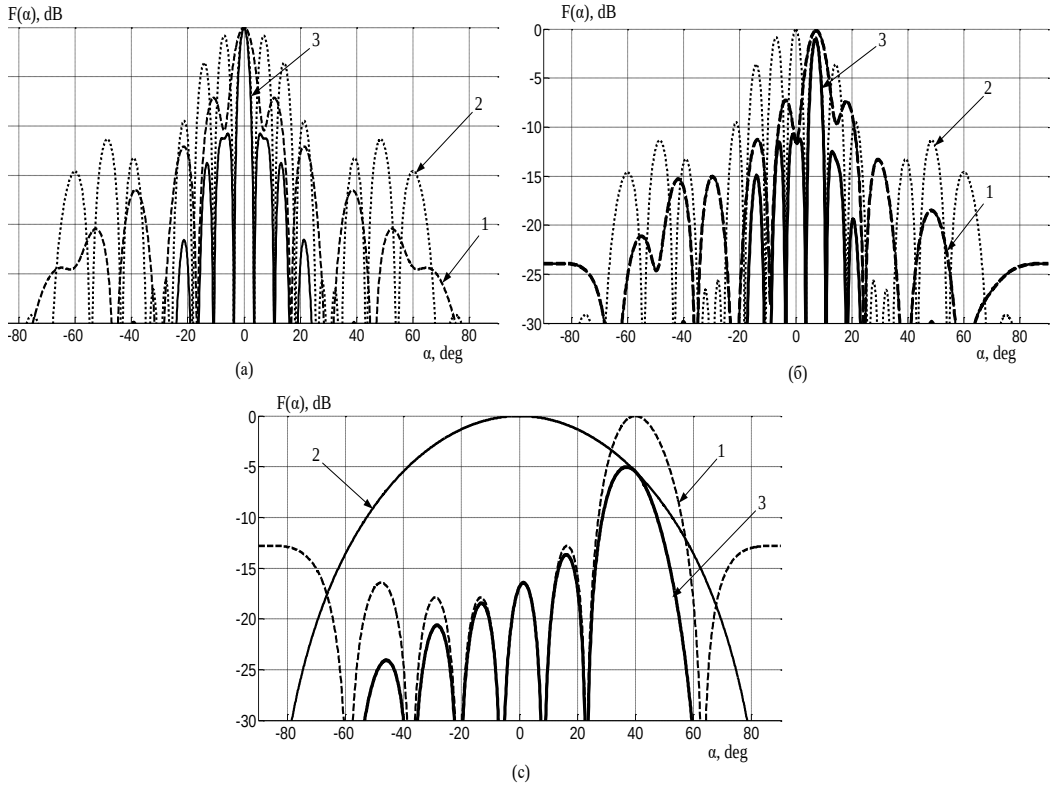

Fig. 7. Antenna directivity pattern using receiving subarrays during beam formation in the direction of (a) – 0°, (b) – 9.5°, (c) – 40° for near zone

In this case, the formation of a narrow beam of the directivity pattern of the receiving array in the azimuth plane is obtained, but interference maximums arise. Non equidistant arrangement of the array elements is known to reduce the interference maximums of the directivity pattern of a sparse antenna array [44]. With the appropriate choice of antenna array architecture, the level of the interference peaks decreases. In our case, we can easily provide different distances

between central part of the receive array and its spaced subarrays. When working in a narrow sector of view in far zone, interference maximums appear in the region of the side lobes of the transmitter's directivity pattern, and in the resulting directivity pattern these maximums are suppressed. To receive signals reflected from objects in the near zone, it is necessary to use a filled antenna array that does not have interference in the entire field of view.

The transmit part of the phased antenna array is placed between the fragments of the receiving array, exactly between its central part and edge parts. To concentrate the energy within the sector of far zone, corresponding transmit array should be wide enough, including from eight to ten columns. At the same time, in the near zone it is possible to use an antenna, consisting of only two elements included with phase shift of 180º, to form a wide viewing sector. The different width of these two transmit arrays defines the non-equidistant placement of the edge receive subarrays. Figure 8 shows the topology with receiving subarrays located at the edges of the aperture.

In the structure presented in Fig. 8, two transmitting and three receiving antennas are used. The transmitting antenna Tx_1 has a beam width of about 15º and irradiates the entire sector of the far zone. The transmitting antenna Tx_2 irradiates the near-sector with a width of at least ± 45°. To receive signals reflected from objects in the near zone, an antenna (antenna array) Rx_1 is used. The elements of this array are located equidistantly in the azimuth plane with a pitch of half wavelength.

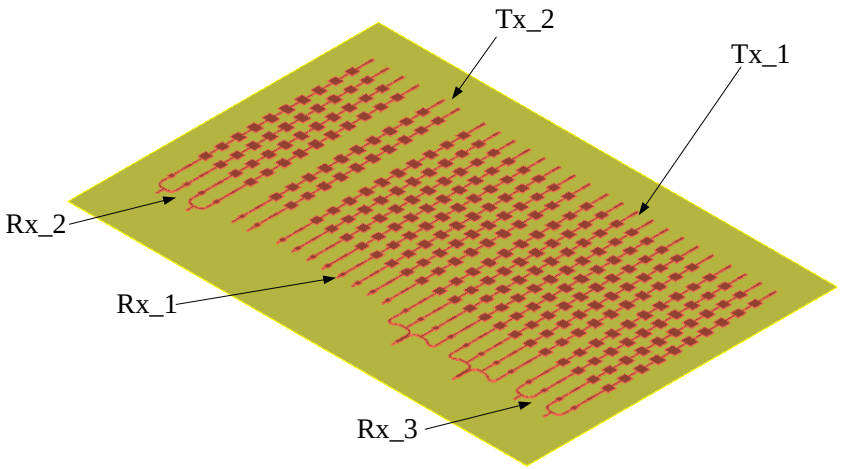

Fig. 8. Structure of the antenna array of the automotive radar

Figure 9 shows the results of electromagnetic modeling of the transmitting array, namely the directivity pattern of the transmitter Tx_1 and the level of matching of its transmitting columns with microstrip transmission lines at the center frequency of the operating range.

The beam width of the transmitter directivity pattern at half power level is 14º in E-plane and 9º in H-plane. The side lobe is -13 dB in E-plane and -15 dB in H-plane. The gain level is about 20 dB.

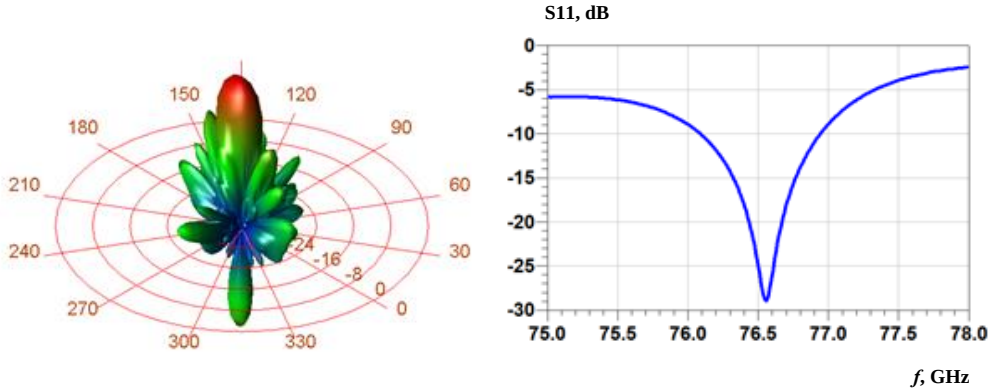

(a) (b)

Fig. 9. The directivity pattern of the transmitter Tx_1 (a) and S11-parameter corresponding to its columns (b)

The far zone antenna can be implemented as a near-field antenna, expanded with additional elements. In this case, the receiving array Rx_1 is used as the central part of the aperture of the receiving antenna for processing the far zone. In addition, two edge antennas Rx_2 and Rx_3 are used. Due to this arrangement of the antenna system, the maximum aperture of the receiving antenna for a given general geometric size is achieved, which ensures the best azimuth resolution. Fig. 10 shows the directivity patterns when placing two subarrays consisting of two columns each one as the edge antenna patterns. Curves 1 and 2 show the transmitting and receiving directivity patterns respectively, curves 3 and 4 show two beams of the resulting directivity pattern, shifted by two degrees relative to each other.

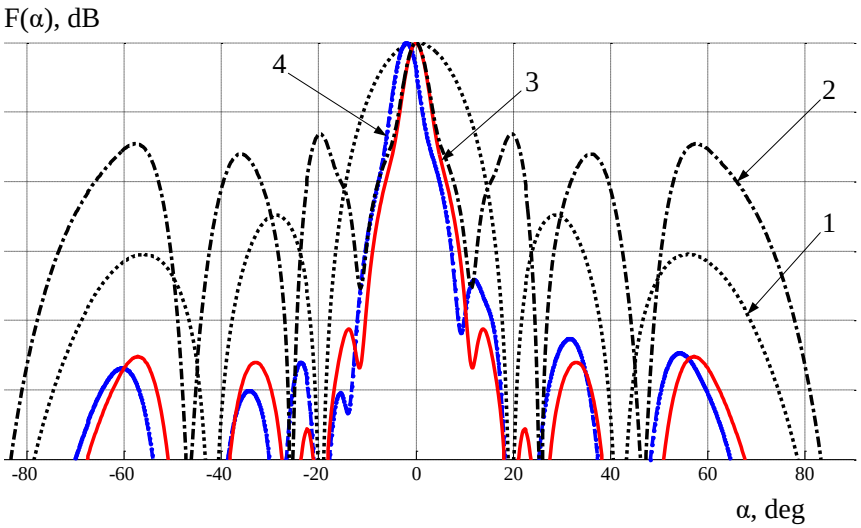

Fig. 10. The transmitting, receiving and resulting antenna directivity patterns with a distributed receiver array structure

The beam width of the resulting directivity pattern in the far zone at half power level is 5°, which is about 1.4 times less than the beam widths with the classic arrangement of the same number of array elements without spacing of receive array fragments. The side lobe level is -20 dB for the center beam and -15 dB for the side beams.

Conclusion

This article discusses the problems of using robotic systems to survey and register tsunami traces in hard-to-reach places. A description of such a complex with good performance characteristics is given. A solution that allows to equip an autonomous mobile robotic complex with a sensor of its own production and increase its cross-country ability is presented. A method for constructing an antenna array is proposed, which makes it possible to achieve close to optimal characteristics with respect to the maximum detection range and angular resolution. It is shown that in comparison with a MIMO antenna consisting of non-overlapping transmitting and receiving apertures, one of which is a sparse array, the proposed configuration provides twice as much power at the receiver output. This result is achieved due to the fact that the entire geometric aperture of the antenna is "filled" with elements (columns) with a step of half of wavelength. Physically, this means that in the case of a sparse aperture, there is a potential possibility to increase the aperture of the receiving antenna and, therefore, the received power. In this case, the placement of the receiving subarrays at the edges of the substrate forms the largest aperture under the conditions of the problem been solved and allows the use of the classical method of beamforming when working in the far zone. An example of constructing an antenna array providing the formation of beams with a width of 5° in the sector of the far-field angles is considered. Application of the proposed solution will expand the detection area of objects. In the future, it is in plan to conduct full-scale tests of automated complexes with an object detection system based on a radar of its own design in the coastal zone of Sakhalin Island.

Acknowledgments

This study has been done in Nizhny Novgorod State Technical University n.a. R.E. Alekseev (NNSTU), and supported by the Agreement № 075-11-2019-053 dated 20.11.2019 (Ministry of Science and Higher Education of the Russian Federation, in accordance with the Decree of the Government of the Russian Federation of April 9, 2010 No. 218), project «Creation of a domestic high-tech production of vehicle security systems based on a control mechanism and intelligent sensors, including millimeter radars in the 76-77 GHz range».

References

1. Titov V., Rabinovich A., Mofjeld H., Thomson R, Gonzalez F. The global reach of the 26 December, 2004 Sumatra tsunami. *Science*. 2005. V. 309. P. 2045-2048.

2. Zaitsev A.I., Kurkin A.A., Levin B.V., Pelinovsky E.N., Yalciner A., Troitskaya Yu., Ermakov S.A. Numerical simulation of catastrophic tsunami propagation in the Indian Ocean (December 26, 2004). *Doklady Earth Sciences*. 2005. V. 402. No. 4. P. 614-618.

3. Choi B.H., Hong S.J., Pelinovsky E. Distribution of runup heights of the December 26, 2004 tsunami in the Indian Ocean. *Geophysical Research Letters*. 2006. V. 33. No. 13. P. L13601.

4. Kim D.C., Kim K.O., Choi B.H., Kim K.H., Pelinovsky E. Three-dimensional runup simulation of the 2004 Indian Ocean tsunami at the Lhok Nga Twin Peaks. *Journal of Coastal Research – SI.* 2013. V. 65. P. 272-277.

5. Gusiakov V.K. Strongest tsunamis in the World Ocean and the problem of marine coastal security. *Izvestiya - Atmospheric and Ocean Physics*. 2014. V. 50. No. 5. P. 435-444.

6. Kim D.C., Kim K.O., Pelinovsky E., Didenkulova I., Choi B.H. Three-dimensional tsunami runup simulation at the Koborinai port, Sanriku coast, Japan. *Journal of Coastal Research – SI*. 2013. V. 65. P. 266-271.

7. Mori N, Takahashi T. The 2011 Tohoku Earthquake Tsunami Joint Survey Group. Nationalwide post event survey and analysis of the 2011 Tohoku Earthquake Tsunami. *Coastal Engineering Journal.* 2012. V. 54. P. 1-27.

8. Choi B.H., Min B.I., Pelinovsky E. Tsuji Y., Kim K.O. Comparable analysis of the distribution functions of runup heights of the 1896, 1933 and 2011 Japanese Tsunamis in the Sanriku Area. *Natural Hazards and Earth System Sciences*. 2012. V. 12. P. 1463-1467.

9. Kaistrenko V., Razjigaeva N., Kharlamov A., Shishkin A. Manifestation of the 2011 Great Tohoku Tsunami on the Coast of the Kuril Islands: A Tsunami with Ice. *Pure and Applied Geophysics*. 2013. V. 170. P. 1103-1114.

10. Gusiakov V.K. *Tsunami history – recorded* / A. Robinson, E. Bernard (Eds.). The Sea, V. 15. Tsunamis. – Cambridge: Harvard University Press, 2009. P. 23-53.

11. Pelinovsky E.N. *Hydrodynamics of tsunami waves*. – N. Novgorod: Institute of Applied Physics of the Russian Academy of Sciences, 1996. 276 p.

12. Zaitsev A.I., Kovalev D.P., Kurkin A.A., Levin B.W., Pelinovsky E.N., Chernov A.G., Yalciner A. The Nevelsk tsunami on August 2, 2007: Instrumental data and numerical modelling. *Doklady Earth Sciences*. 2008. V. 421. No. 1. P. 867-870.

13. Zaitsev A.I., Kovalev D.P., Kurkin A.A., Levin B.V., Pelinovskii E.N., Chernov A.G., Yalciner A. The tsunami on Sakhalin on August 2, 2007: Mareograph evidence and numerical simulation. *Russian Journal of Pacific Geology*. 2009. V. 3. No. 5. P. 437-442.

14. Levin B.W., Kaistrenko V.M., Rybin A.V., Nosov M.A., Pinegina T.K., Razzhigaeva N.G., Sasorova E.V., Ganzei K.S., Ivel'skaya T.N., Kravchunovskaya E.A., Kolesov S.V.,

Evdokimov Yu.V., Bourgeois J., MacInnes B., Fitzhugh B. Manifestations of the tsunami on November 15, 2006, on the central Kuril Islands and results of the runup heights modelling. *Doklady Earth Sciences*. 2008. V. 419. No. 1. P. 335-338.

15. Laverov N.P., Lobkovsky L.I., Levin B.W., Rabinovich A.B., Kulikov E.A., Fine I.V., Thomson R.E. The Kuril tsunamis of november 15, 2006, and january 13, 2007: Two trans-pacific events. *Doklady Earth Sciences*. 2009. V. 426. No. 1. P. 658-664.

16. Lobkovsky L.I., Rabinovich A.B., Kulikov E.A., Ivashchenko A.I., Fine, I.V., Thomson R.E., Ivelskaya T.N., Bogdanov G.S. The Kuril Earthquakes and tsunamis of November 15, 2006, and January 13, 2007: Observations, analysis, and numerical modeling. *Oceanology*. 2009. V. 49. No. 2. P. 166-181.

17. Shevchenko G., Ivelskaya T., Loskutov A., Shishkin A. The 2009 Samoan and 2010 Chilean tsunamis recorded on the Pacific coast of Russia. *Pure and Applied Geophysics*. 2013. V. 170. P. 1511-1527.

18. Dotsenko S.F. The Black Sea tsunamis. *Izvestiya - Atmospheric and Oceanic Physics*. 1995. V. 30. No. 4. P. 483-489.

19. Yalciner A., Pelinovsky E., Talipova T., Kurkin A., Kozelkov A., Zaitsev A. Tsunamis in the Black Sea: comparison of the historical, instrumental and numerical data. *Journal of Geophysical Research*. 2004. V. 109. No. C12. P. C12023.

20. Zaitsev A.I., Pelinovsky E.N. Forecasting of tsunami wave heights at the Russian coast of the Black Sea. *Oceanology*. 2011. V. 51. No. 6. P. 907-915.

21. Dotsenko S.F., Kuzin I.P., Levin B.V., Solov'eva O.N. Tsunami in the Caspian sea: Seismic sources and features of propagation. *Oceanology*. 2000. V. 40. No. 4. P. 474-482.

22. Didenkulova I.I., Pelinovsky E.N. Phenomena similar to tsunami in Russian internal basins. *Russian Journal of Earth Sciences*. 2006. V. 8. No. 6. P. ES6002-1-9.

23. Didenkulova I.I., Pelinovsky E.N. Phenomena like the tsunami in Russian internal reservoirs. *Fundamentalnaya i Prikladnaya Gidrofizika*. 2009. No. 3(5). P. 52-64.

24. Torsvik T., Paris R., Didenkulova I., Pelinovsky E., Belousov A., Belousova M. Numerical simulation of tsunami event during the 1996 volcanic eruption in Karymskoe lake, Kamchatka, Russia. *Natural Hazards and Earth System Sciences*. 2010. V. 10. P. 2359- 2369.

25. Farreras S. *Post-tsunami survey field guide* IOS. Manuals and Guides, No. 30. – Paris: UNESCO, 1998. 45 p.

26. Pelinovskij E.N. International expeditions for Tsunami. *Bulletin of Russian Foundation for Basic Research*. 1996. No 5. P. 26-30.

27. Fritz H.M., Synolakis C/E., Kalligeris N., Skanavis V., Santoso F.J., Rizal M., Prasetya G.L.Y., Liu Ph.L-F. The 2018 Sulawesi tsunami: field survey and eyewitness video analysis using lidar. *Geophysical Research Abstracts*. 2019. V. 21. P. 1-1.

28. Zaytsev A., Belyakov V., Beresnev P., Filatov V., Makarov V., Tyugin D., Kurkin A. Coastal monitoring of the Okhotsk sea using an autonomous mobile robot. *Science of Tsunami Hazards*. 2017. V. 36. No. 1. P. 1-12.

29. Kurkin A., Tyugin D., Kuzin V., Zeziulin D., Pelinovsky E., Malashenko A., Beresnev P., Belyakov V. Development of a group of mobile robots for conducting comprehensive research of dangerous wave characteristics in coastal zones. *Science of Tsunami Hazards*. 2018. V. 37. No. 3. P. 157-174.

30. Kurkin A.A., Tyugin D.Y., Kuzin V.D., Chernov A.G., Makarov V.S., Beresnev P.O., Zeziulin D.V. Autonomous mobile robotic system for environment monitoring in a coastal zone. *Procedia Computer Science*. 2017. V. 103. P. 459-465.

31. Beresnev P.O., Kurkin A.A., Tyugin D.Y., Orlov I.Y., Filatov V.I., Belyakov V.V. Experimental study of autonomous complexes motion. *Proceedings of the Fourteenth MEDCOAST Congress on Coastal and Marine Sciences, Engineering, Management and Conservation*. 2019. V. 2. P. 881-891.

32. Dickmann J., Appenrodt N., Bloecher H.-L., Brenk C., Hackbarth T., Hahn M., Klappstein J., Muntzinger M., Sailer A. Radar contribution to highly automated driving. *Proceedings of the European Radar Conference*. Rome. Italy. 2014. P. 412–415.

33. Myakinkov A.V., Sidorov S.B., Shishanov S.V., Shabalin S.A. The distributed radar system for monitoring the surrounding situation for the intelligent vehicle. *Proceedings of the 19th Int. Radar Symposium*. Bonn. Germany. 2018. P. 1-8.

34. Pirkani A.A., Pooni S., Cherniakov M. Implementation of MIMO beamforming on an OTS FMCW automotive radar. *Proceedings of the Int. Radar Symposium*. 2019. 8 p.

35. Engels F., Wintermantel M., Heidenreich P. Automotive MIMO radar angle estimation in the presence of multipath. *Proceedings of the European Radar Conference*. 2017.

36. Rohling H., Meinecke M.-M. Waveform Design Principles for Automotive Radar System. *Proceedings of the CIE Int. Conference on Radar*. 2001.

37. Shabalin S.A., Myakinkov A.V., Kuzin A.A., Ryndyk A.G. Millimeter-wave Phased Antenna Array for Automotive Radar. *Proceedings of the 20th Int. Radar Symposium*. Ulm. Germany. 2019. P. 1-8.

38. Scolnik M.I. *Radar handbook*. Third edition. The McGraw-Hill Companies. 2008.

39. Amin M.G., Belouchrani A., Zhang Y. The spatial ambiguity function and its applications. *IEEE Signal Processing Letters*. 2000. V. 7. Issue: 6.

40. Rohling H., Moller C. Radar waveform for automotive radar systems and applications. *Proceedings of the Radar Conf. 2008 RADAR'08*. Rome. Italy. 2008. P. 1–4.

41. Jasteh D., Gashinova M., Hoare E.G., Tran T.-Y., Clarke N., Cherniakov M. Low-THz Imaging Radar for Outdoor Applications. *Proceedings of the 16th Int. Radar Symposium*. 2015. V. 1. P. 203-208.

42. Vizard D.R, Gashinova M., Hoare E.G., Cherniakov M. Low-THz Automotive Radar Developments Employing 300-600 GHz Frequency Extenders. *Proceedings of the 16th Int. Radar Symposium*. 2015. V. 1. P. 209-214.

43. Zwanetski A., Kronauge M., Rohling H. Waveform Design for FMCW MIMO Radar Based on Frequency Division. *Proceedings of the 14th Int. Radar Symposium*. 2013. V. 1. P. 89-94.

44. Shabunin S.N., Chechetkin V.A., Klygach D.S., Ershov A.V., Vakhitov M.G., Dumchev V.A., Dumchev I.A. Non-equidistant antenna array with low level of side lobes. *Proceedings of the 2016 IEEE 6th Int. Conference on Communications and Electronics*. 2016. P. 230-233.